Electric field related extinction reduction in diffraction experiments on α-LilO 3

J. Bouillot, J. Baruchel, M. Remoissenet, J. Joffrin, J. Lajzerowicz

Classification
Physics Abstracts
61.12D — 61.70B

Electric field related extinction reduction in diffraction experiments on α-$LiIO_3$

J. Bouillot (*), J. Baruchel (**), M. Remoissenet (***), J. Joffrin (****) and J. Lajzerowicz (*****)

(*) I.L.L., 156X, 38042 Grenoble Cedex, France.
(**) Laboratoire Louis Néel, C.N.R.S., associé à l'U.S.M.G., 166X, 38042 Grenoble, France.
(***) Laboratoire d'Optique du Réseau Cristallin, Faculté des Sciences, Dijon, France.
(****) Sans domicile scientifique fixe.
(*****) Laboratoire de Spectrométrie Physique, U.S.M.G., Grenoble, France.

(*Reçu le 10 août 1981, révisé les 4 novembre 1981 et 1er avril 1982, accepté le 23 avril 1982*)

Résumé. — Une importante réduction de l'extinction a été observée précédemment lors d'expériences de diffraction de neutrons sur des cristaux de α-$LiIO_3$, lorsqu'un champ électrique était appliqué suivant l'axe **c**. Nous avons étudié des échantillons produits dans des conditions de croissance différentes, par diffraction des neutrons et des rayons γ et par topographies aux rayons X et aux neutrons, dans le but de mieux expliquer cet effet. Nous avons pu montrer que le phénomène est causé par une augmentation de la distorsion du réseau cristallin dans certaines zones du cristal. Un modèle qualitatif, basé sur une accumulation de charges dans ces zones, et sur les propriétés de conduction ionique et piézoélectriques du matériau, permet d'expliquer nos observations.

Abstract. — A strong reduction of the extinction of α-$LiIO_3$, previously reported in neutron diffraction, when an electric field is applied along the **c**-axis, is studied in more detail in this paper to improve the understanding of this phenomenon. Neutron and γ-ray diffraction measurements, and neutron and X-ray diffraction topography experiments are performed on samples produced under various growth conditions. The results suggest that the enhancement of the distortion in some crystal regions could be due to an accumulation of charges in these regions. This mechanism is mainly driven by the ionic conductivity and the piezoelectricity of the crystal.

1. **Introduction.** — α-$LiIO_3$ crystals (hexagonal space group $P6_3$) show pyroelectricity along the *c*-axis and strong anisotropic piezoelectricity. They have been widely used for their non-linear optical properties [1]. In recent years this material was also investigated for some other special properties : anomalous dielectric behaviour and nearly one-dimensional ionic conductivity along the *c*-axis [2, 3]. In addition, another peculiar behaviour was recently observed : the neutron intensity diffracted using the 0002 Bragg reflection, for instance, can be enhanced several times under the effect of a moderate electric D.C. field along the *c*-axis [4]. The authors of this observation reached the following conclusions :

- The observed diffracted intensity enhancement, or in other words, the reduction of extinction, is temperature dependent ;
- the reduction is field dependent and the effect for the 0004 reflection is much smaller than for the 0002 reflection ;
- an anomalous enhancement of the light diffraction pattern is also reported and is explained in terms of space charge decoration of quasi periodic layer defects [5] ;
- an explanation was proposed [6] based on a phenomenological model which infers that space charges of different nature accumulate at defects of macroscopic scale and produce a gradient of lattice parameters : the mosaic spread of the crystal is correspondingly increased. A similar diffraction effect was also observed in quartz [7] when a strong external electric field was applied.

The purpose of the experimental study reported below is to explain how and why this reduction of extinction under the influence of a D.C. electric field can be observed in α-$LiIO_3$ crystals. To achieve this we have performed several new experiments which include neutron diffraction intensity measurements using different Bragg peaks, X-ray and neutron topography experiments at several temperatures, and a careful study of the mosaic spread of the crystal using a good resolution γ diffractometer.

2. **Sample characteristics.** — The samples are platelets cut perpendicular to the *a*-axis (sample S3d) or *c*-axis (the other samples). Five samples were mainly investigated. Sample S1 was grown at the Institute of Physics of the Academia Sinica of Peking ([1]). Samples S2 and S3a, b, c and d were cut from crystals grown by ourselves [8] from aqueous solutions with respective pH values 2 and 6 (see also reference [9]); sample S2 was cut from the growth pyramid of a single crystal obtained with a relatively high growth rate (3 times faster than the usual rate); the S3 samples, grown under optimal conditions, have a very good crystal quality. An optical polish was easily performed on S2 and S3, whereas an attempt to polish S1 was unsuccessful; this suggests that important defects, probably inclusions, are present in the S1 sample. The thickness is 0.4 mm for S3c and 2.5 mm for all the others. In order to investigate the field effect, evaporated gold or silver paste electrodes were deposited on the large faces of the platelets.

3. **Overall diffraction experiments.** — 3.1 NEUTRON DIFFRACTION. — Using a neutron spectrometer, the intensity of the 0002 Bragg reflection was measured as a function of the electric field applied along the *c*-direction. Figure 1 shows the experimental curves corresponding to sample S1, with different electric fields. The full width at half maximum (FWHM) is

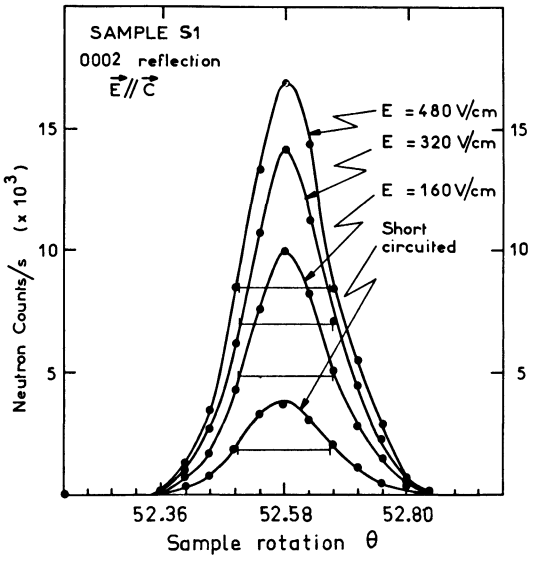

Fig. 1. — 0002 rocking curves of sample S1 for different electric fields applied along the *c*-axis (wavelength $\lambda \sim 3$ Å).

electric field independent and is just the resolution of the spectrometer. The peak centre positions do not vary when the electric field is applied, but the maximum intensity is strongly electric field dependent.

([1]) Kindly provided by Prof. Yang-Chen from Peking Institute of Physics.

This is also shown in figure 2 where additional measurements performed on samples S2 and S3a are reported. The various results will be discussed later. When the electric field is removed, and the sample short circuited, a few hours are necessary for the sample to return to its previous situation. All these results are in total agreement with those already published [4].

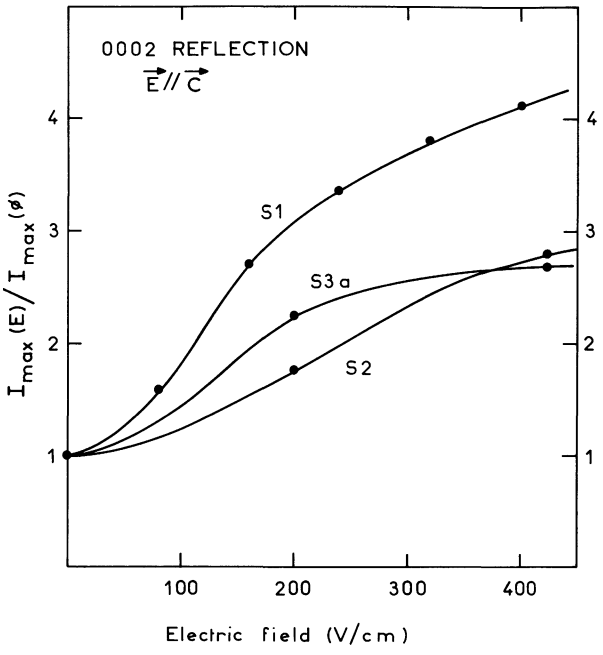

Fig. 2. — Electric field dependence of the ratio $I_{max}(E)/I_{max}(0)$, using the 0002 Bragg reflection for different samples, where $I_{max}(E)$ is the maximum peak intensity for an electric field E applied parallel to the *c*-axis.

3.2 γ-RAY DIFFRACTION. — 3.2.1 *Instrumental aspect* [10]. — The instrument consists of the γ source (an irradiated gold foil), a beam-defining slit, the goniometer and a NaI scintillation counter (Fig. 3).

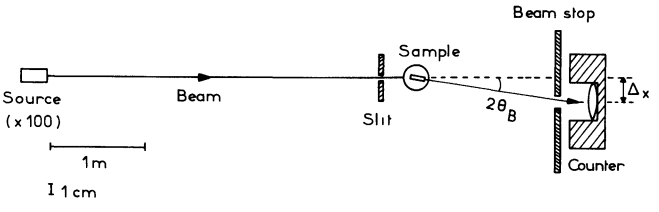

Fig. 3. — γ-ray spectrometer.

The wavelength of the beam is 0.030 8 Å, its horizontal divergence nearly 20″ and its size 10 mm high and 0.2 mm broad. The rotation mechanism of the sample table can produce steps of 2″ around the vertical axis. The counter is fixed in Δx position corresponding to a calculated Bragg reflection. The shape of the rocking curve of an imperfect crystal gives information in the following way :

a) From a comparison between the measured integrated reflection power R_{meas} and the theoretical values R_{kin} and R_{dyn} corresponding to the kinematic and dynamical theories respectively, we obtain an estimate of the degree of perfection of the sample.

b) From the FWHM of the reflected beam, one can get the mosaic spread distribution in different volume elements of the sample.

3.2.2 *Experimental results.* — When no electric field is applied, the rocking curves corresponding to the volume illuminated by the beam, i.e. to a 0.2 mm thick crystal slice and to the 0002 reflection, give a mosaic spread which is about 20″ for all the investigated samples. This is nearly the γ-spectrometer resolution and is independent of the location of the slice in the sample; it evidences the high crystal quality of the samples. Let us note that the Darwin width for γ-rays is very small, less than 1″ of arc and does not appear in our measurements. When an electric field is applied, the occurrence of tails on both sides of the peak is sometimes observed. This effect depends on the sample (various qualities) and it is strongly dependent on the scattering region (inhomogeneity). On figure 4, one of the most important observed effects is shown. The diffraction peak can be well separated into two contributions where the first one always exists and is just the experimental width (it corresponds to the perfect parts of the crystal), whereas the second one increases with the applied field and its profile is clearly non Gaussian (it corresponds to non perfect parts of the crystal). Figure 5 represents rocking curves obtained for different slice positions from one electrode to the other. The shape and the intensity of the peaks depend strongly on the position in the sample.

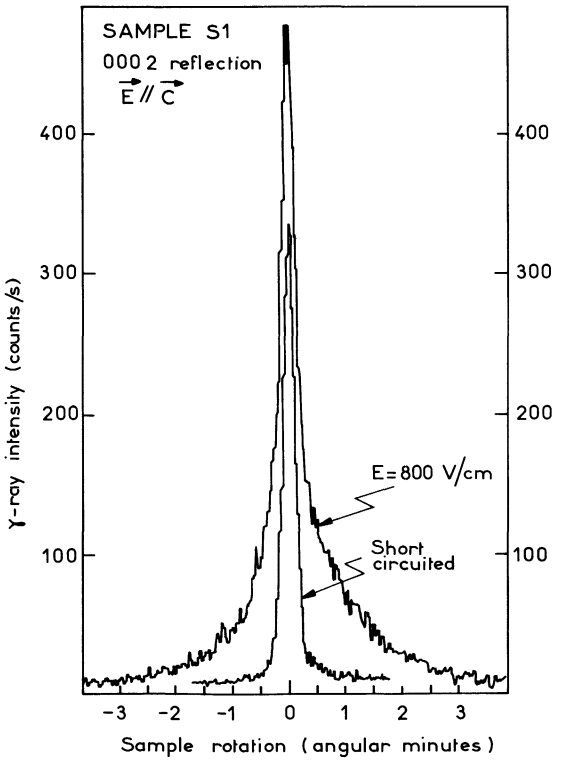

Fig. 4. — Electric field effect on the γ-ray intensity of the 0002 Bragg reflection when sample S1 is rotated (rocking curves).

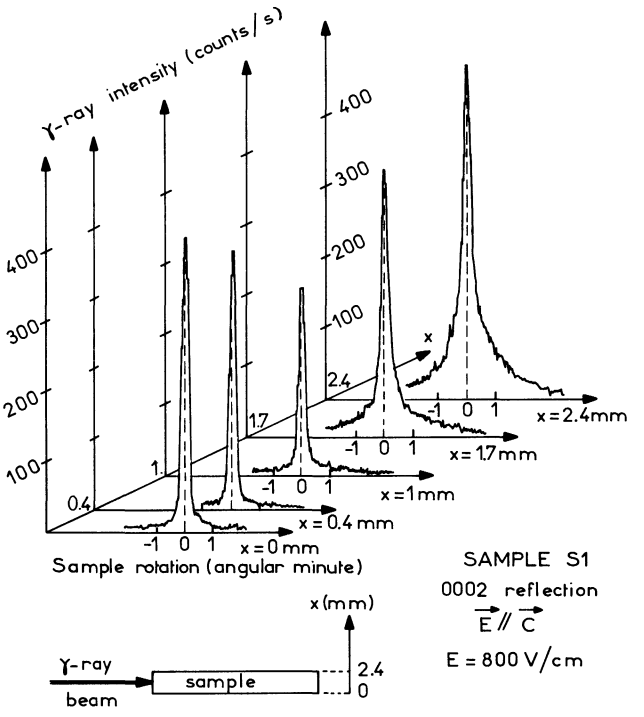

Fig. 5. — Position (x) dependence of the rocking curves measured with the 0002 Bragg reflection of sample S1, an electric field being applied along the c-axis.

As previously observed in neutron diffraction experiments, the integrated intensity of the rocking curve slowly decreases with time when the sample is short circuited. Moreover, when the sample is heated up to 350 K, the electric field effect disappears.

4. Local diffraction experiments : X-ray and neutron diffraction topography. — 4.1 X-RAY AND NEUTRON DIFFRACTION TOPOGRAPHY. — Topographic techniques [11] are simply the local counterpart of usual X-ray or neutron diffraction measurements. In these last cases the sample is completely illuminated by the incident beam, and scattered intensities are recorded as a whole; any spatial variations of the diffracted beam intensity are thus averaged out. X-ray or neutron diffraction topography try to recover this wasted information. From an experimental point of view they consist essentially in setting the single crystal sample for a chosen Bragg reflection, and placing an X-ray or neutron sensitive photographic detector across the diffracted beam. Crystal inhomogeneities (defects, domains, ...) can give rise to local variations of Bragg reflectivity, hence to contrast

within the investigated Bragg spot, which thus becomes an image of the specimen. The main contrast mechanism in neutron topography, as well as in the low absorption case in X-ray topography (when $\mu t \lesssim 1$, where μ is the absorption coefficient and t the thickness of the sample) is the so called « kinematical image » one [12]. The crystal lattice is distorted in the neighbourhood of an inhomogeneity; if this distortion affects the reflecting planes being used, this region will Bragg-diffract components of the incident beam that would not participate to diffraction if the crystal were perfect : in other words, extinction is reduced.

This intensity transfer from the transmitted to the diffracted beam direction leads to a locally *enhanced* blackening on the photographic plate, i.e. *white* contrast with the photographic reproduction scheme used in the work.

X-ray and neutron diffraction topography appear as complementary tools in the present investigation. The resolution on the topographs is about one order of magnitude better in the X-ray case (~ 4 μm instead of ~ 60 μm). On the other hand the small absorption of neutrons by lithium iodate (the absorption coefficient μ is 118 cm^{-1} in the Mo Kα X-ray case, while $\mu \simeq 0.9$ cm^{-1} for neutrons of $\lambda \simeq 1.5$ Å) allows the investigation of the behaviour of a crystal slice extending from one electrode to the other to be made as a function of the applied electric field in rather thick samples ($t \sim 2.5$ mm), by using neutron diffraction *section* topography [13]. The beam width is then restricted to less than the crystal thickness (Fig. 6), and only a virtual slice of the sample contributes, as a first approximation, to the diffraction. In this way only inhomogeneities contained in this slice give rise to contrast on the resulting topograph, the edges of which are associated with the entrance and exit surfaces respectively.

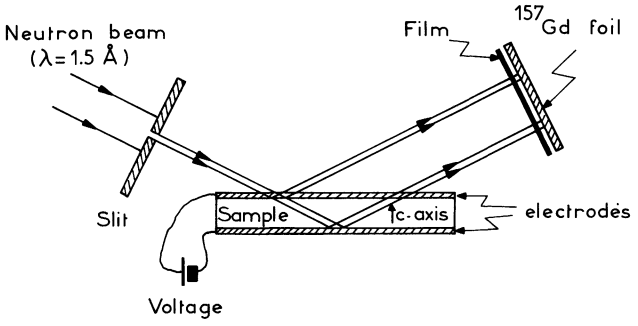

Fig. 6. — Neutron diffraction section topography experimental arrangement.

X-ray topographs were performed using a rotating anode generator with a Mo anode, while neutron topographs were made on the I.L.L. instrument S20, a small diffractometer mainly devoted to topography, located at the end of a curved thermal neutron guide. The neutron beam was monochromatized ($\lambda \sim 1.5$ Å, monochromatic beam intensity $\sim 3 \times 10^4$ neutrons cm^{-2} s^{-1}) using the 111 reflection from a Cu crystal with a mosaic spread of 7'. X-ray topographs were recorded on L4 25 μ Ilford nuclear plates, whereas X-ray dental film (Kodak Periapical Ultra Rapide) backed by a ^{157}Gd foil acting as a (n_β) converter, was used in the neutron case. The neutron direct monochromatic beam width was restricted to ~ 0.7 mm, leading to exposure times of 15 h. We call the topograph performed using the *hkjl* Bragg reflection « *hkjl* topograph ».

4.2 Experimental results. — Figure 7 shows two $\bar{3}122$ X-ray topographs of sample S3c which only differ by the applied electric field :

a) short circuited and *b*) 1.4 kV/cm. On the first topograph, 7*a*, the main features are surface scratches

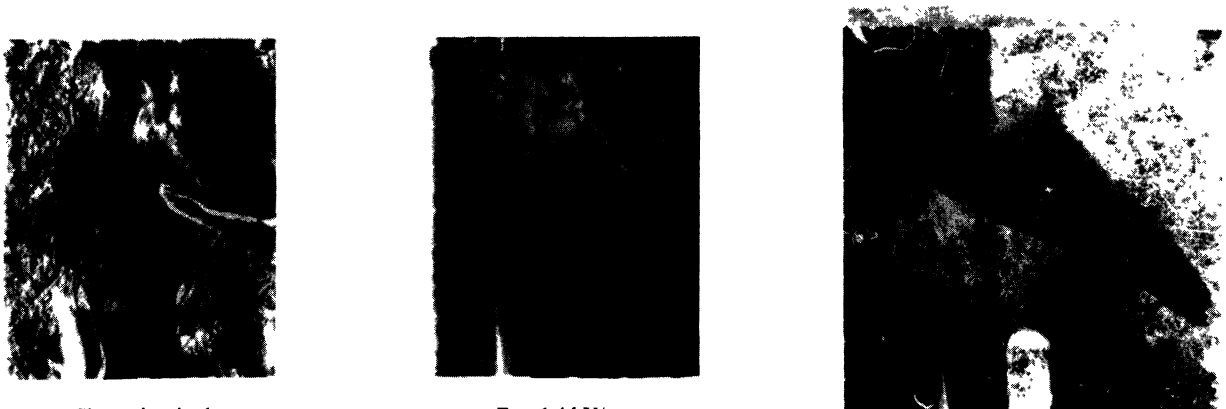

Short circuited
(*a*)

E = 1.4 kV/cm
(*b*)

electrode
(*c*)

SAMPLE S3b $\bar{3}122$ reflection E// c

Fig. 7. — X-ray topographs of sample S3c using the $\bar{3}122$ Bragg reflection : the projection of the diffraction vector is horizontal. The main sample surfaces are (0001) planes : *a*) sample short circuited; *b*) electric field applied parallel to the *c*-axis (X7.7); *c*) photograph of one electrode after applying the electric field (X9).

whereas on the topograph of figure 7*b* area contrast is observed between different regions of the sample, indicating that they are distorted in different ways. The photograph of figure 7*c* shows that some areas of one of the evaporated gold electrodes (the cathode), which were visually bright before the application of the electric field, become dull, the other electrode remaining unaffected. This is probably related to the earlier observation [14, 15] that lithium accumulates on the cathodic surface of the sample, and is simply associated with ionic conduction. Now a correlation between the dull surfaces (white areas on figure 7*c*) and the less illuminated regions of figure 7*b* is straightforward : the inhomogeneous distortion is therefore associated with an inhomogeneous ionic conductivity along the *c*-axis, less conducting regions appearing as the more distorted. Some of the observed defects are weakly visible on the topograph 7*a*. But the same effect occurs on other samples, where the surface is less distorted, and where nearly no defect is visible by Lang's method of X-ray topography [11] when no field is applied.

In order to clarify why the conductivity is inhomogeneous, on the one hand, and whether the observed effect is a bulk or surface phenomenon, on the other hand, we have carried out neutron diffraction section topographs (NDST). Figure 8 shows three 0002 NDST of sample S3b which again only differ by the applied electric field : *a*) short circuited *b*) + 2 kV/cm and *c*) − 2 kV/cm. The thickness of the investigated samples was bigger than in the X-ray case (~ 2.5 mm instead of 0.4 mm). No special care was taken in order to prevent surface distortions; this explain, at least partly, the enhanced diffracted intensity of the surface images with respect to the bulk of the sample. As in all NDST shown, the exit surface appears less illuminated than the entrance surface simply because of the absorption associated with Li. The geometry of our experiment is such (Fig. 6) that the diffracted beam coming from the entrance surface does not travel in the sample volume, whereas that corresponding to the exit surface suffers absorption, μl being ~ 1.5, where l is the beam path within the crystal.

The comparison of figures 8*b* and *c*, and figure 8*a* shows, in agreement with the previous measurements, that the diffracted beam intensity rises when the electric field is applied. But they also reveal that this increase is neither homogeneous across the sample volume nor localized near the electrodes only; it appears as a strong enhancement of the visibility of defects. The width and shape of the main images show that they are associated with growth bands [16]. The visible growth bands are not always the same when the field is reversed. This lack of symmetry is not unexpected since the pyroelectric polarization of the material is not affected by the applied field.

Figure 9 shows the way in which the observed reduction of extinction takes place in sample S2.

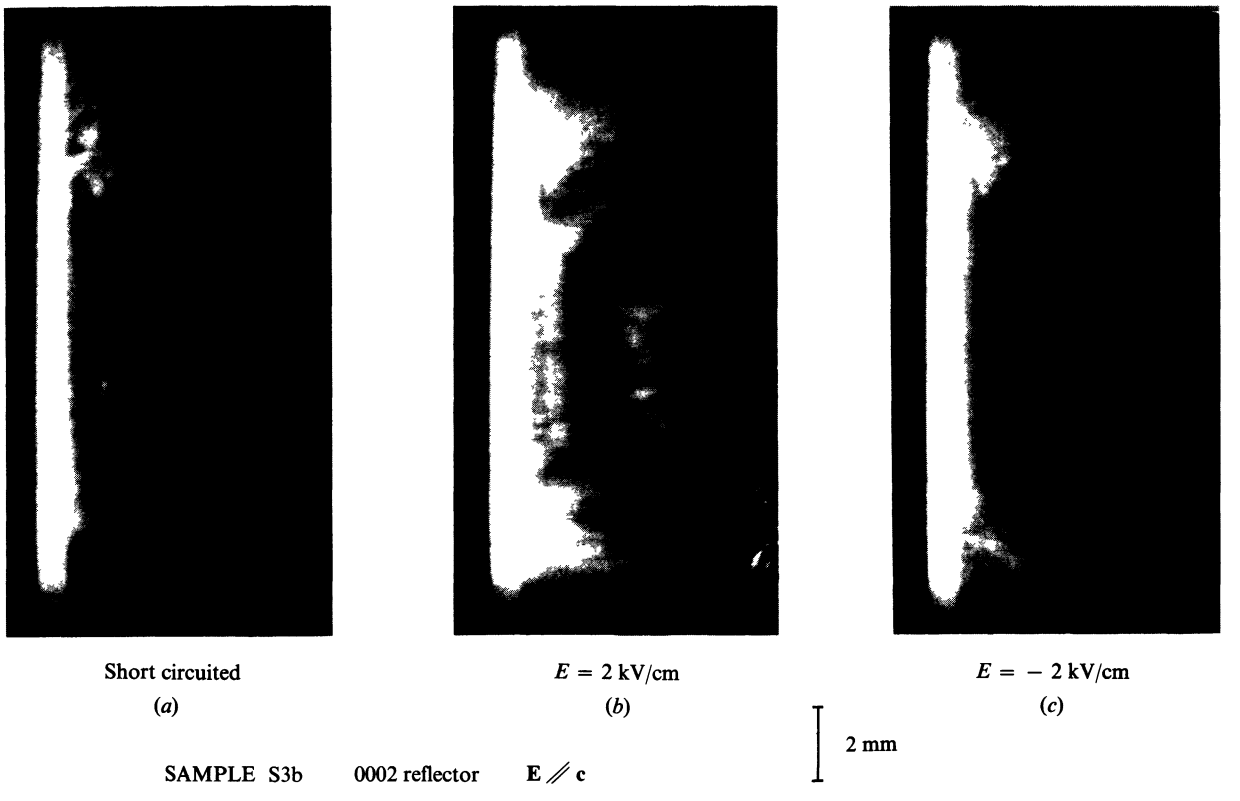

Fig. 8. — Neutron topographs of sample S3b using the 0002 Bragg reflection for different applied electric field conditions. The main surfaces of the crystal are perpendicular to the *c*-axis (horizontal on the topograph).

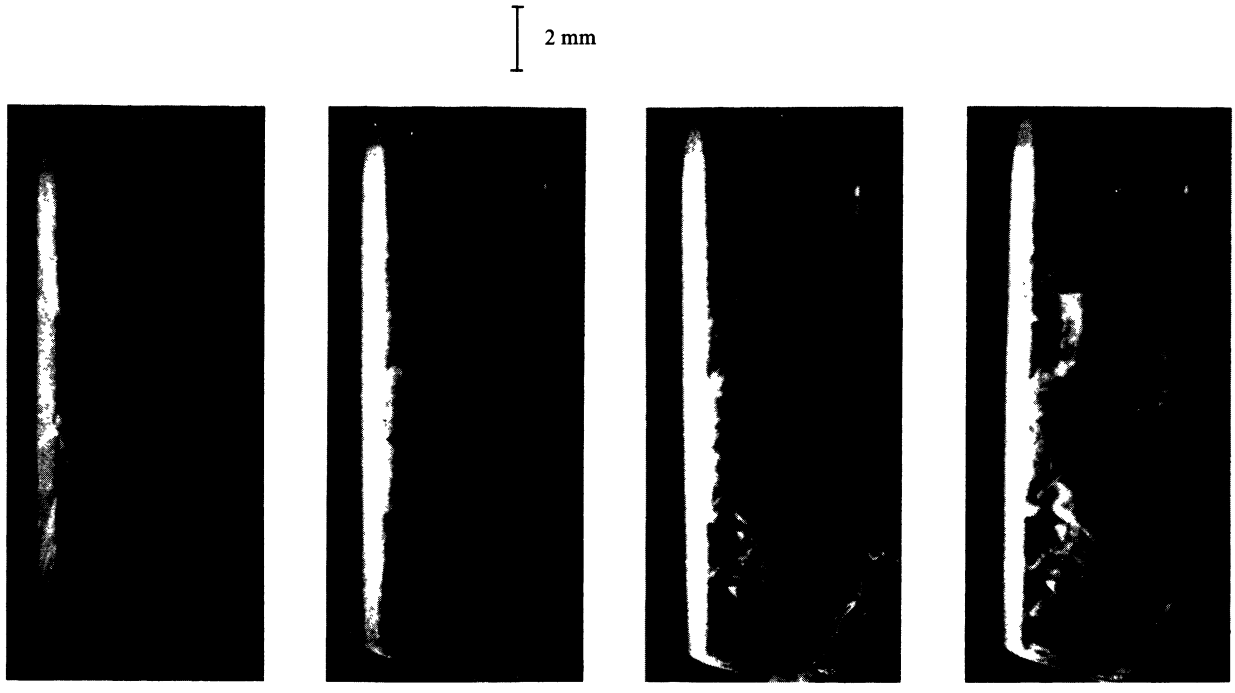

Fig. 9. — Neutron topographs of sample S2 using the 0002 Bragg reflection for increased electric field applied along the c-axis. The diffraction vector is horizontal.

The electric field was increased from 0 to 120 V/cm in steps of 40 V/cm. The images of the surfaces remain nearly constant. There is no spatial extension of the distorted regions but a steadily rising enhancement of the intensity diffracted from the same locations, associated with an increasing lattice distortion.

These distorted regions are not related, in this case, with growth bands, but probably with another kind of inhomogeneities, perhaps inclusions. When the (0001) surfaces of the sample are only partially covered by electrodes, the effect we are concerned with only occurs in the regions where an electric field parallel to **c** is present. When a field of the same magnitude is applied along **a**, on the sample S3d, only an extremely faint effect, independent of the sign of the electric field, is observed.

We have investigated the effect using the $3\bar{3}00$ reflection. The field was 4 times stronger than when investigating the 0002 reflection, but maintained along the c-axis; the topograph shows a very weak inhomogeneous enhancement of diffracted intensity.

Another hint that the ionic conductivity is a crucial parameter of the problem, as will be discussed in more detail in the next section, are the low and high temperature topographs we have performed. When a field, big enough to produce a strong effect at room temperature, is applied at $T \sim 170$ K, no variation is observed on the 0002 topograph. On the other hand, if the field is applied at room temperature before cooling the sample, and removed at 170 K, the low temperature topograph is identical to that obtained at room temperature in an applied field, indicating that the distortion effect remains during a time much bigger than the exposure time. When the sample is warmed to 354 K the applied field only produces a weak enhancement of the 0002 diffracted intensity, and the inner part of the section topograph appears nearly homogeneous.

5. **Discussion.** — This discussion is a first attempt to explain the observations reported. Our main purpose was to find a model in agreement with the experimental results, and any other explanation which reaches the same aim is obviously to be considered. In this sense, this paper tries to make some progress comparatively to the one already published on the quartz [7]. A complete theoretical model is not yet possible because of the complicated character of this crystal which is both piezoelectric and pyroelectric. Moreover the region where defects occur have no simple geometry. Therefore the following discussion is mainly qualitative.

In order to know what the extinction of our samples is when no electric field is applied, the experimental values of the integrated reflecting power (I.R.P.) for γ-rays or neutrons are compared to the theoretical values, calculated from both the dynamical and kinematic theories of diffraction [17] (see Table I). The results show that for the dimensions of the studied α-$LiIO_3$ platelets neutrons and γ-rays are equivalent

Table I.

	$R^{0002}_{\text{dynamical}}$ —	$R^{0002}_{\text{measured}}$ —	$R^{0002}_{\text{kinematic}}$ —
γ-rays ($\lambda = 0.030\,8$ Å)	0.6×10^{-7}	10^{-5}	10^{-4}
Neutrons ($\lambda \cong 1.5$ Å)	5×10^{-6}	10^{-4}	10^{-3}

from an extinction investigation point of view, i.e. $R_{\text{meas}}/R_{\text{kin}}$ is nearly the same in both cases. This occurs in spite of the fact that the extinction period is about 8 times bigger in the γ-ray case, because the apparent thickness of the sample is also about 8 times bigger in this case. For the X-ray case the calculation was not performed because it is complicated due to the absorption effect which cannot be neglected. On the other hand, topographs performed on various samples when no field is applied show nearly no defect. This suggests that our sample defects are neither dislocations nor growth bands or inclusions associated with detectable lattice distortions, with the technique we have used. Only a distribution of small defects is in agreement with the observation; they will be called simply « defects » in the following discussion.

When an electric field is applied parallel to the *c*-axis, a reduction of extinction is observed in some particular regions of the samples. This effect is bigger for $000l$ reflections than for $h\bar{h}00$. Moreover, there is no effect if the electric field is applied perpendicular to the *c*-axis. It can be noticed here that the symmetry of the gradient of distortion (which induces the reduction of extinction) is the same as that of the piezoelectric effect, and this suggests that both physical phenomena are related. The piezoelectric coefficients are [18] :

$$d_{33} = 46 \times 10^{-12}\ \text{CN}^{-1} \quad (000l \text{ distortion}, E /\!/ c)$$

$$d_{31} = 3.7 \times 10^{-12}\ \text{CN}^{-1} \quad (h\bar{h}00 \text{ distortion}, E /\!/ c)$$

$$d_{13} = 0 \quad (000l \text{ distortion}, E \perp c).$$

For comparison, the value for quartz is : $d_{33} = 2.3 \times 10^{-12}\ \text{CN}^{-1}$.

But a perfect piezoelectric crystal would present, under uniform electric field, a homogeneous distortion over the whole sample. Another mechanism must therefore be invoked to intrepret the inhomogeneity of the effect and the fact that an observable reduction of extinction occurs implies a gradient of lattice distortions.

The observed inhomogeneity may be associated with crystal areas where defects have more chance to exist, as for instance those resulting from perturbation during the crystal growth. At this step of the discussion, the ionic conductivity, which is another important property driving the mechanism, must be introduced. This ionic conductivity ($\sigma_c = 10^{-8}\,\Omega^{-1}\,\text{m}^{-1}$ and $\sigma_c/\sigma_a = 5 \times 10^2$ at room temperature [3], which is small compared with $10^{-2}\ \Omega^{-1}\ \text{cm}^{-1}$ for a good ionic conductor) can be considered as one-dimensional. The ionic carriers are mainly the Li^+ ions [14, 15]. Our experiments have shown an electrolysis which is consequently attributed to a deposit of lithium. Moreover, this deposit only exists in the regions where no reduction of extinction is observed on the topographs (dark regions). A possible explanation is that Li-ions, moving under applied electric field action, are trapped in the neighbourhood of a defect. This decoration of defects implies an accumulation of Li-ions on one side of the defect and of Li-vacancies on the other side. It results in a strong local internal electric field parallel to the *c*-axis (10^8 V/m is the order of magnitude starting from crude considerations). The local lattice distortion induced by the anisotropic piezoelectric effect can reach values of the order of 10^{-2} for $\Delta c/c$ and 10 times smaller for the other lattice parameter. It should decrease with distance from the decorated defect and become negligible ($\lesssim 10^{-6}$) when the distance is about 0.1 μm (elastic calculation in the case of simple geometries). Since the resolution of the topographs varies from about 5 to 60 μ, the gradient of lattice distortion cannot be observed in the case of an isolated defect. Therefore, one must assume that these defects are distributed with a mean distance of less than 0.1 μ, over regions of 5 to 60 μ size at least.

It is of interest to notice here that if the lattice distortion was only due to the elastic effect of the accumulation of Li-ions in the vicinity of defects (without taking into account piezoelectricity), the observed effect should be nearly isotropic because of the associated elastic constants :

$$C_{11} = 8.3 \times 10^{10}\ \text{Nm}^{-2}$$

and

$$C_{33} = 5.7 \times 10^{10}\ \text{Nm}^{-2} \quad [19].$$

Since it is not, we are justified in concluding that the elastic contribution is much smaller than the piezoelectric contribution.

When the external electric field is reversed, the intensity of the effect changes probably because of the pyroelectric nature of the crystal [20]; some topographs even show that the occurrence of the enhanced contrast can correspond to different regions of the sample.

When the electric field is applied perpendicular to the *c*-axis, no effect is observed, in agreement with the fact that, first, the concerned piezoelectric coefficient is zero, and, second, the ionic conductivity is about 500 times smaller than that parallel to the *c*-axis.

When the crystal is cooled, the Li-ions motion is frozen in such a way that (i) the effect does not appear if the electric field is applied at low temperature (170 K), and that (ii) once the electric field is applied at room temperature, the effect remains at low tempe-

rature, even if the electric field is removed after cooling down.

When the crystal is heated (354 K), no clear effect can be observed because the Li-ions are sufficiently thermally activated to overcome the potential barriers due to the defects. This is in accordance with the increasing of conductivity along the *c*-axis [3]. Let us note that the transverse ionic conductivity cannot play a role because it remains nearly constant in the considered temperature range [3].

Room temperature seems to be a good compromise for this crystal, as far as this effect is concerned. It makes this crystal more suitable than others which can exhibit the same effect.

Our tentative explanation can thus be summarized as follows : the observed effect occurs when a suitable distribution of defects, which varies from one sample to the other, is present in the crystal, and this effect is driven both by the nearly one-dimensional weak ionic-conductivity and the very large piezoelectricity of the material. It is now clear that the observed effect does not take place only near the electrodes, as was suggested earlier [6].

This explanation could also apply to quartz which exhibits the same effect when applying a much larger electric field [7]. Indeed, both ionic conductivity (mainly due to impurities) and piezoelectricity exist, but are much smaller than in our case. A similar effect exists in KDP and DKDP which shows a correlation between the location of the conductivity inhomogeneities and the position of the crystal defects, using X-ray transmission topographs [21]. Finally, samples without piezoelectric effects ($LiKSO_4$, TiO_2, NaCl...) have been investigated, and no effect occurs [4].

Let us note that an alternative explanation is also conceivable : the pyroelectric polarization could be compensated within small but nevertheless macroscopic volumes of the crystal by charged defects. Moreover, as these charges compensate the elastic distortion associated with the defects, the action of the field would be, in this assumption, to make the defects free of charges, leading then to a decrease of extinction and to an enhanced visibility of defects in topographs. But, on the one hand, the phenomenon is more likely to occur in other crystals, and that has not been observed, and, on the other hand, this explanation is not in agreement with the occurrence of Li deposit on the cathodic side of the higher crystalline quality regions of the sample (Fig. 7).

The next step to make progress in understanding this electric field effect is to know the nature of the assumed defects and to follow the dynamics of the phenomenon. Concerning the first point, time dependent X-ray topograph using a high flux has also been performed, but additional experiments using other Bragg reflections and different exposure times are necessary to get more details concerning the defects. As for the second aspect (dynamical), the integrated reflections measured as a function of time when the electric field is switched on and off, as well as the electrical measurement of charge flow which shows the same time dependence do not give enough additional information to improve the proposed model, but do not contradict it. Further experiments are in progress in these domains.

Acknowledgments. — We are grateful to M. Schlenker for helpful discussions, and to B. Michaux for growing crystals and preparing different kinds of samples.

References

[1] NASH, F. R., BERGMAN, J. G., BOYD, G. D. and TURNER, E. N., *J. Appl. Phys.* **40** (1969) 5201.

[2] ARLT, G., PUSCHERT, W. and QUADFLIED, P., *Phys. Status Solidi* (a) **3** (1970) K 243.

[3] REMOISSENET, M., GARANDET, J. and AREND, H., *Mat. Res. Bull.* **10** (1975) 181.

[4] YANG-CHEN, NIN-SHIWEN and CHENG-YU-FEN, *Sci. Sin.* **XXII** (1979) 1000.

[5] XU-ZHENG-TI, LI-TIE-CHENG and GU-BEN-YUAN, *Acta Phys. Sin.* (1979) 28-894 and
YANG HUA GUANG, LI CHEN-XI and XU ZHENG-YI, *Acta Phys. Sin.* **30** (1981) 928.

[6] HU-HUA-CHEN, *J. Physique-Lett.* **42** (1981) L-189.

[7] YAMASHITA, S. and KATO, N., *J. Appl. Crystallogr.* **8** (1975) 623.

[8] AREND, H., REMOISSENET, M. and STAEHLIN, W., *Mat. Res. Bull.* **7** (1972) 869.

[9] ADVIENKO, K. E., KYDAROV, B. E. and SHELAPOT, D. V., *J. Cryst. Growth* **42** (1977) 228.

[10] SCHNEIDER, J. R., *J. Appl. Crystallogr.* **7** (1974) 541.

[11] See for instance MALGRANGE, C. and SCHLENKER, M. and BARUCHEL, J., in « Imaging Processes and Coherence in Physics », *Lecture Notes in Physics* (Springer-Verlag, Berlin) **112** (1980) 302 and 320.

[12] AUTHIER, A., *Adv. in X-ray Analysis* **10** (1967) 9.

[13] SCHLENKER, M., BARUCHEL, J., PERRIER DE LA BATHIE, R. and WILSON, S. A., *J. Appl. Phys.* **46** (1975) 2845.

[14] VLOKH, O. G., VELICHKO, I. A. and LAZ KO, L. A., *Sov. Phys. Crystallogr.* **20** (1975) 263.

[15] LUTZE, R., GIESEKE, W. and SCHRÖLER, W., *Solid State Commun.* **23** (1977) 215.

[16] KLAPPER, H., in « *Characterization of Crystal Growth Defects by X-ray Methods* », edited by B. K. Tanner and D. K. Bowen, Nato Advanced Study Institutes Series (Plenum Press, N.Y.) **B 63** (1980) 133.

[17] ZACHARIASEN, W. H., *Theory of X-ray diffraction in crystals* (John Wiley, N.Y.) 1945.

[18] HAUSSÜHL, S., *Phys. Status Solidi* **29** (1968) K 159.

[19] Measurements not yet published.

[20] LIMINGA, R. and ABRAHAMS, S. C., *J. Appl. Crystallogr.* **9** (1976) 42.

[21] BELOUET, C. and MONNIER, M., *Acta Electronica* **18** (1975) 143.